Supplementary Information

Dopant ion concentration-dependent upconversion luminescence of cubic $SrF_2:Yb^{3+},Er^{3+}$ nanocrystals prepared by a fluorolytic Sol-Gel method

Melissa-Jane Monks, Christian Würth, Erhard Kemnitz and Ute Resch-Genger

A. SrF_2:Yb,Er UCNC dispersions - Doping series

Table S1. Employed reactant amounts of precursor cations and methanolic HF for the preparation of 20 mL $Sr_{1-(x+y)}Yb_xEr_yF_{2+(x+y)}$-sol.

Stoichiometry	Abbreviation	χ_{Yb} [%]	χ_{Er} [%]	n_{Sr} [mmol]	n_{Yb} [mmol]	n_{Er} [mmol]	n_{HF} [mmol]
$Sr_{0.94}Yb_{0.05}Er_{0.01}F_{2.06}$	**5-1**	5	1	3.76	0.2	0.04	8.32
$Sr_{0.89}Yb_{0.10}Er_{0.01}F_{2.11}$	**10-1**	10	1	3.56	0.4	0.04	8.51
$Sr_{0.84}Yb_{0.15}Er_{0.01}F_{2.16}$	**15-1**	15	1	3.36	0.6	0.04	8.71
$Sr_{0.74}Yb_{0.20}Er_{0.01}F_{2.21}$	**20-1**	20	1	3.16	0.8	0.04	8.9
$Sr_{0.93}Yb_{0.05}Er_{0.02}F_{2.07}$	**5-2**	5	2	3.72	0.2	0.08	8.32
$Sr_{0.88}Yb_{0.10}Er_{0.02}F_{2.12}$	**10-2**	10	2	3.52	0.4	0.08	8.51
$Sr_{0.83}Yb_{0.15}Er_{0.02}F_{2.17}$	**15-2**	15	2	3.32	0.6	0.08	8.71
$Sr_{0.78}Yb_{0.20}Er_{0.02}F_{2.22}$	**20-2**	20	2	3.12	0.8	0.08	8.9
$Sr_{0.92}Yb_{0.05}Er_{0.03}F_{2.08}$	**5-3**	5	3	3.68	0.2	0.12	8.32
$Sr_{0.87}Yb_{0.10}Er_{0.03}F_{2.13}$	**10-3**	10	3	3.48	0.4	0.12	8.51
$Sr_{0.83}Yb_{0.15}Er_{0.03}F_{2.18}$	**15-3**	15	3	3.28	0.6	0.12	8.71
$Sr_{0.77}Yb_{0.20}Er_{0.03}F_{2.23}$	**20-3**	20	3	3.08	0.8	0.12	8.9

Table S2: Yb^{3+}, Er^{3+} and Sr^{3+} amounts (χ_{Yb}, χ_{Er}, χ_{Sr}) determined by ICP-OES of series χ_{Er} = 1 % and χ_{Er} = 2 %. The ratios were met with small deviations. Sample 10-1 shows the highest deviation with χ_{Yb} = 13.5 % instead of χ_{Yb} = 10 %.

sample	χ_{Yb}	χ_{Er}	χ_{Sr}
5-1	5.4	1.0	93.6
10-1	13.5	1.3	85.2
15-1	15.0	1.0	84.0
20-1	20.9	1.0	78.1
5-2	5.2	1.9	92.9
10-2	9.7	1.8	88.5
15-2	14.4	1.8	83.9
20-2	19.3	1.8	78.9

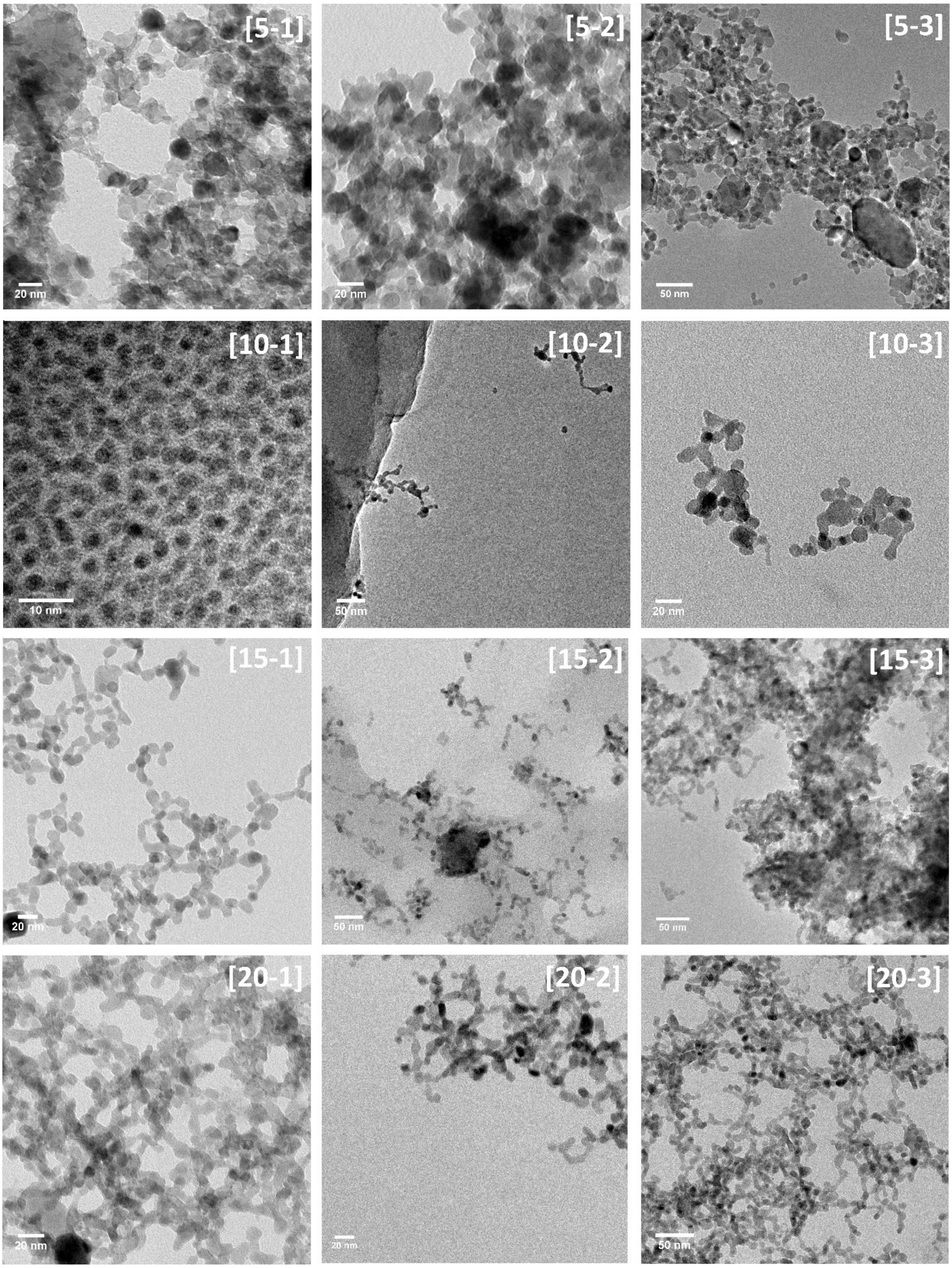

Figure S3: TEM images of SrF_2:Yb,Er UCNC dispersions of the doping series. Er^{3+}-amount (χ_{Er}) left to right 1 %, 2 %, 3 %; Yb^{3+}-amount (χ_{Yb}) top to bottom 5 %, 10 %, 15 %, 20 %.

Table S4: Integration intervals of electronic transitions.

notation	Electronic	Integration interval

	transition	[nm]
blue	$^2H_{9/2} \rightarrow {}^4I_{15/2}$	394.0 – 430.0
green	$^2H_{11/2} \rightarrow {}^4I_{15/2}$	507.0 – 533.6
	$^4S_{3/2} \rightarrow {}^4I_{15/2}$	533.6 – 580.0
Red	$^4F_{9/2} \rightarrow {}^4I_{15/2}$	630.0 – 685.0
NIR1	$^4I_{9/2} \rightarrow {}^4I_{15/2}$	780.0 – 833.0
NIR2	$^4S_{3/2} \rightarrow {}^4I_{13/2}$	833.0 – 880.0
total UC		394.0 – 880.0

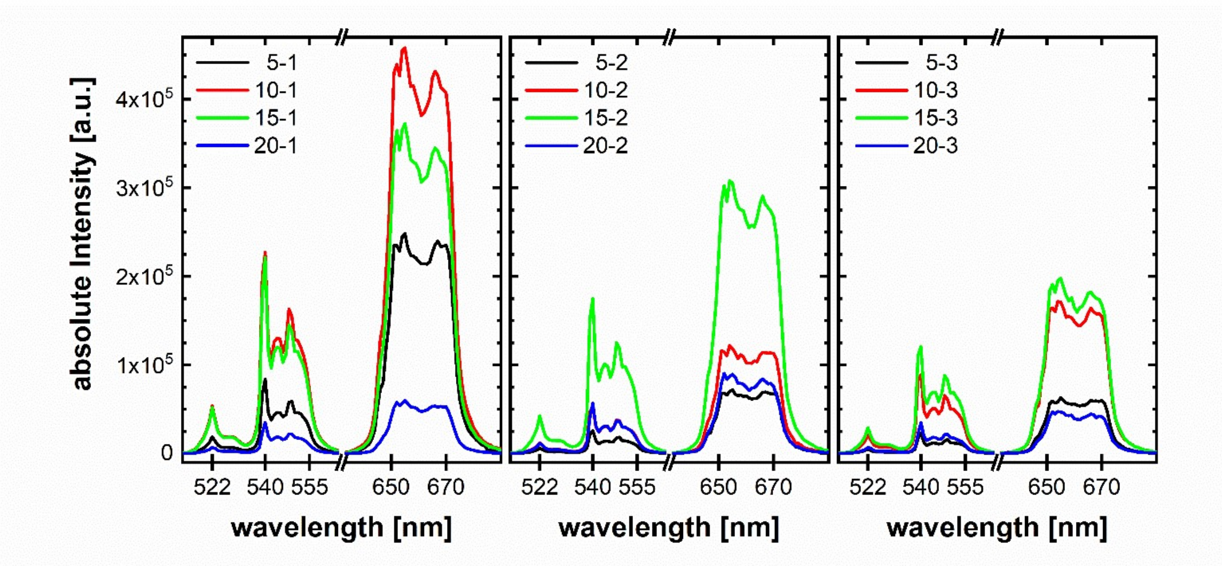

Figure S5: Absolutely measured UCL spectra of the green- and red-emitting transition ($^2H_{11/2}$, $^4S_{3/2} \rightarrow {}^4I_{15/2}$, and $^4F_{9/2} \rightarrow {}^4I_{15/2}$) at the varied doping amounts. For clarity, the spectra are divided into three groups according to the Er^{3+}-amount (χ_{Er}). The most evident result is the much higher total UCL intensity at particularly low χ_{Er} of 1%. An increase in χ_{Er} to 2 % and 3 % yields gradually lower intensity.

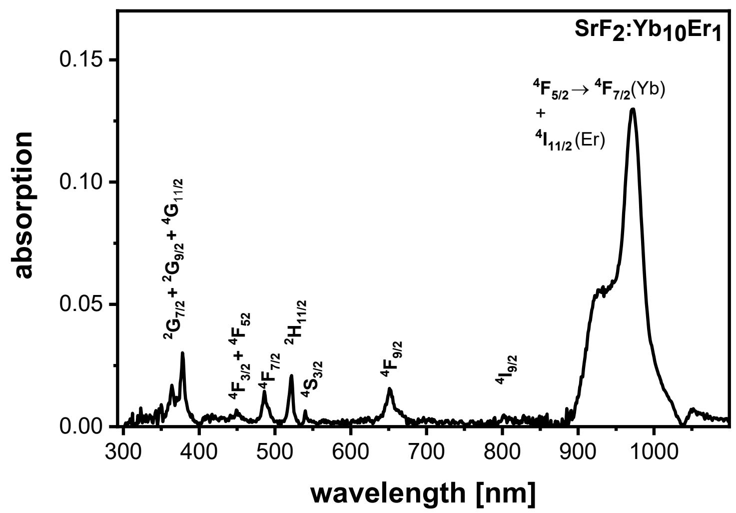

Figure S6: Absorption spectrum of SrF_2:$Yb_{10}Er_1$ powder obtained via reflectance/transmission measurements.

Calculation of relative brightness

The nanocrystal brightness (B_{UCNC}) is the Brightness of an individual UCNC. B_{UCNC} is calculated from the product of the UCL quantum yield (Φ_{UCL}), the absorption cross section of the sensitizer (σ_{Yb}) and the number of sensitizer species within an average UCNC ($N_{Yb,UCNC}$). $N_{Yb,UCNC}$ can be calculated from the product of the number of unit cells (N_{unit}) within a single UCNC and the fraction of cells containing a sensitizer ion (sensitizer doping amount, χ_{Yb}). The number of unit cells is the fraction of the volume (V_{UCNC}) of an individual UCNC and the volume of a unit cell (V_{unit}). For comparing of the resulting values we use the relative brightness (B_{rel}) which is the quotient of B_{UCNC} to the brightness of the best performing UCNC ($B_{UCNC,max}$*). Using eq. S1, eq. S2 and eq. S3, eq. S4 can be derived which was used for calculation of B_{rel}.

$$B_{UCNC} = \Phi_{UCL} \cdot \sigma_{Yb} \cdot N_{Yb,UCNC} \qquad \text{eq. S1}$$

$$N_{Yb,UCNC} = N_{unit} \cdot \chi_{Yb} = \frac{V_{UCNC}}{V_{unit}} \cdot \chi_{Yb} \qquad \text{eq. S2}$$

$$B_{rel} = \frac{B_{UCNC}}{B_{UCNC,max}{}^{*}} \qquad \text{eq. S3}$$

$$B_{rel} = \frac{\Phi_{UCL} V_{UCNC} \cdot \chi_{Yb}}{\Phi_{UCL}^{*} V_{UCNC}^{*} \cdot \chi_{Yb}^{*}} \qquad \text{eq. S4}$$

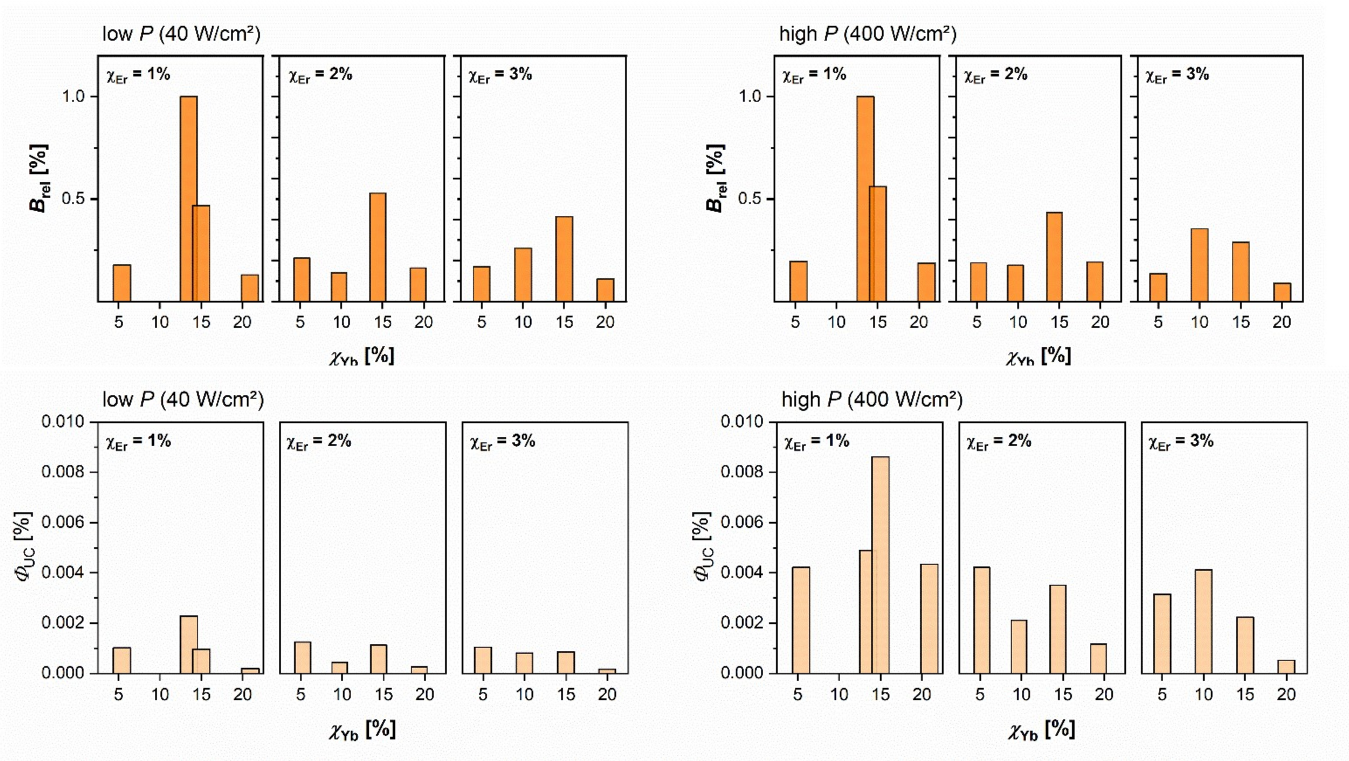

Figure S7: Relative brightness (top) and upconversion quantum yield (Φ_{UC}) determined for low and high excitation power density (low P = 40 W/cm², high P = 400 W/cm²); of SrF_2:Yb,Er UCNC dispersions in ethylene glycol (λ_{ex}= 980 nm) at varied χ_{Er} (1 %, 2 % 3 %) and χ_{Yb} (5 % ,10 % ,15 %, 20%)

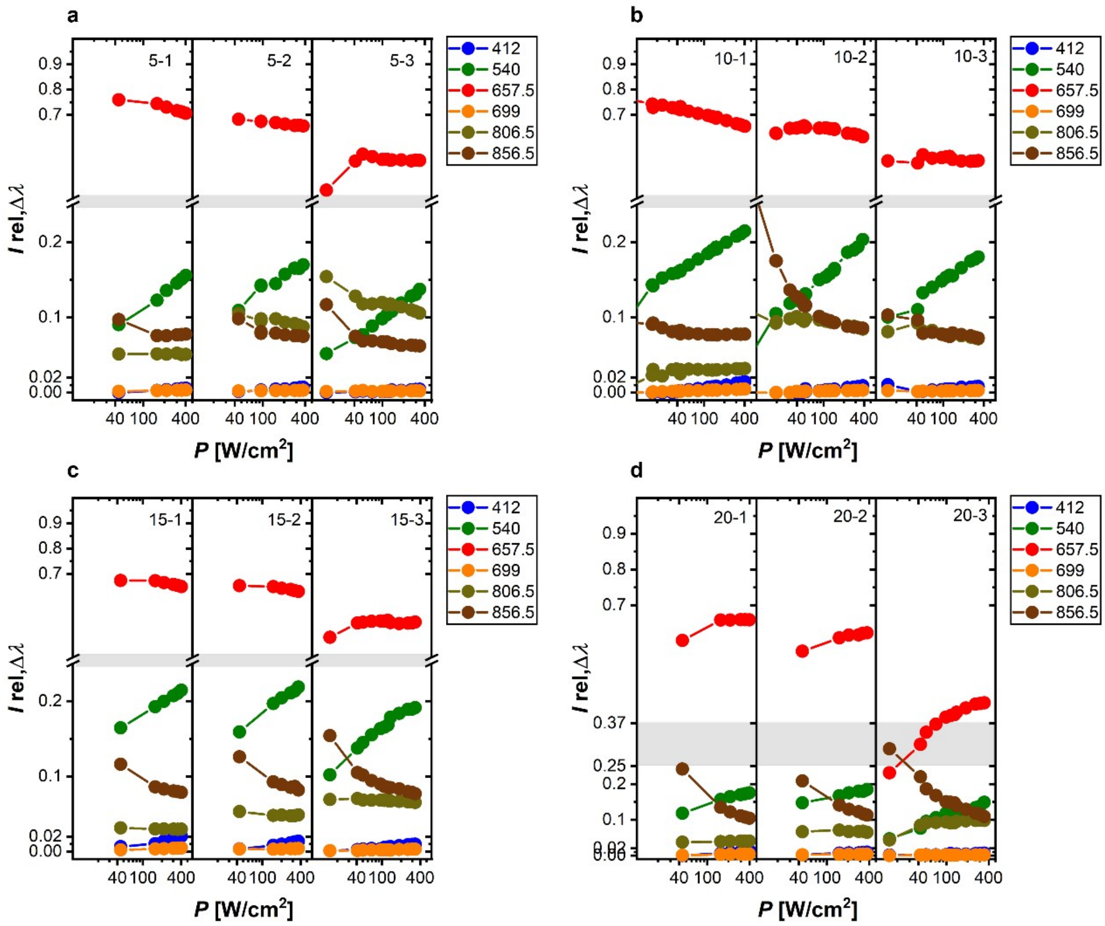

Figure S8: *P*-dependent relative spectral UCL distribution ($I_{rel,\Delta\lambda}(P)$) of $SrF_2{:}Yb_xEr_y$ UCNC dispersions in ethylene glycol (λ_{ex}= 980 nm) at varied χ_{Yb} (5 %, 10 %, 15 %, 20%) and χ_{Er} (1 %, 2 % and 3 %). Grouped by Yb^{3+} amount **(a)** χ_{Yb} = 5% **(b)** χ_{Yb} = 10% **(c)** χ_{Yb} = 15% **(d)** χ_{Yb} = 20%; The panels in each figure χ_{Er} from left to right: 1 %, 2 % and 3 %.

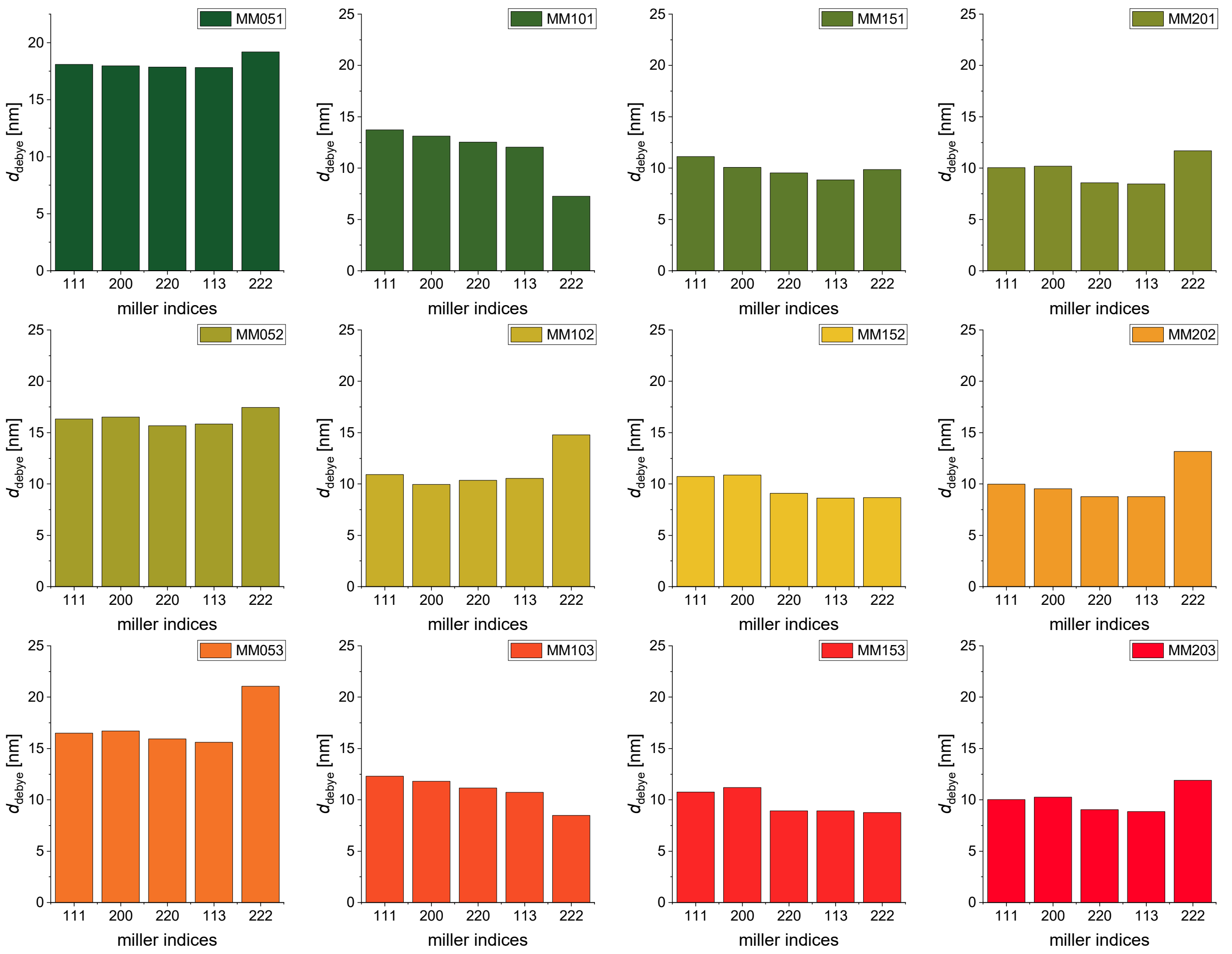

Figure S9: Crystallite size obtained by the *Debye-Scherrer* equation: values mentioned in the text are mean values of the crystallite sizes calculated of 5 different lattice planes [(111), (200), (220), (113), (222)].

B. SrF_2:Yb,Er UCNC Xerogels - Calcination series

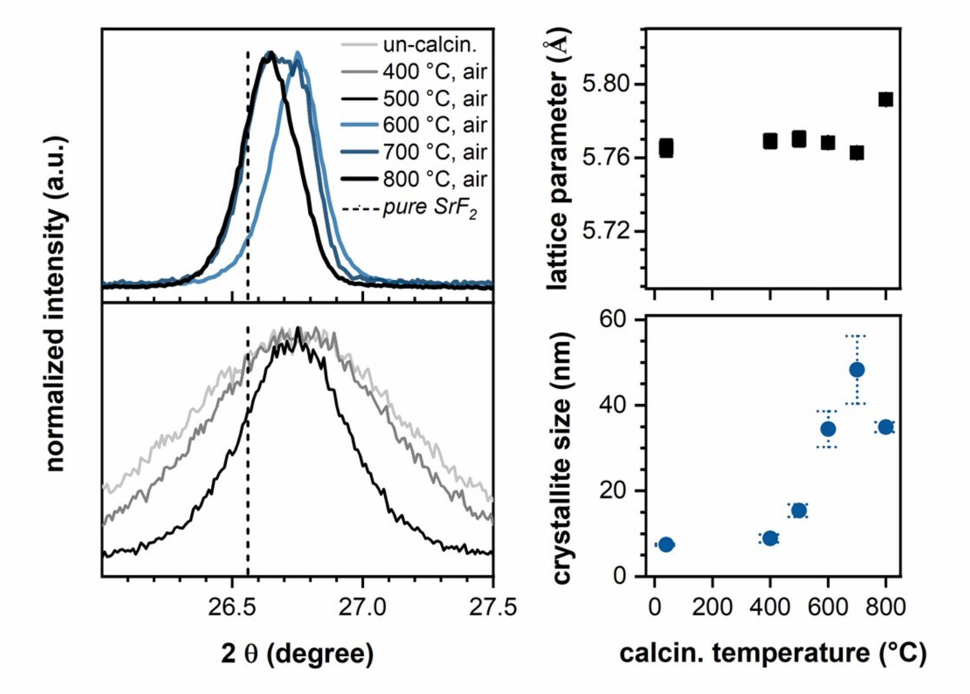

Figure S10: (111) reflection at 26.7° (left); lattice parameter (right, top), crystallite size (right, bottom) of calcinated UCNC powders.

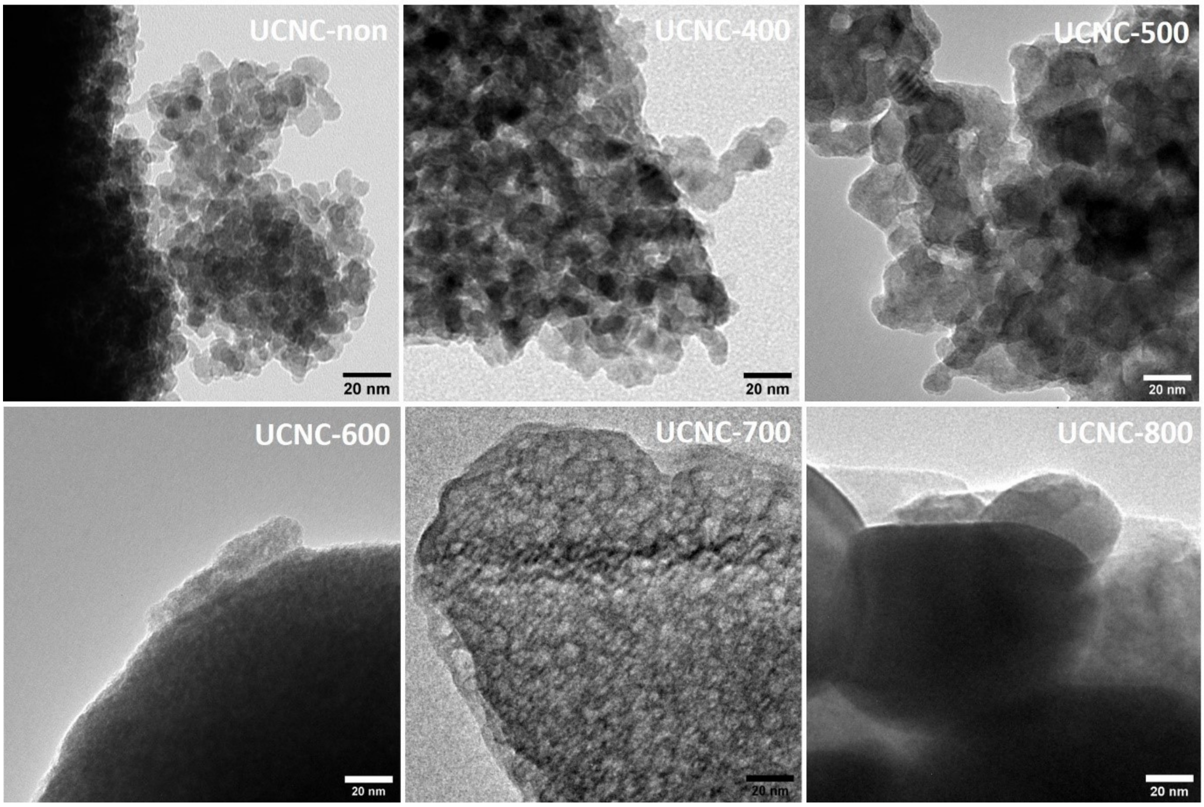

Figure S11: TEM images of UCNC xerogels calcinated at different temperatures (UCNC-non, UCNC-400, UCNC-500, UCNC-600, UCNC-700, UCNC-800).

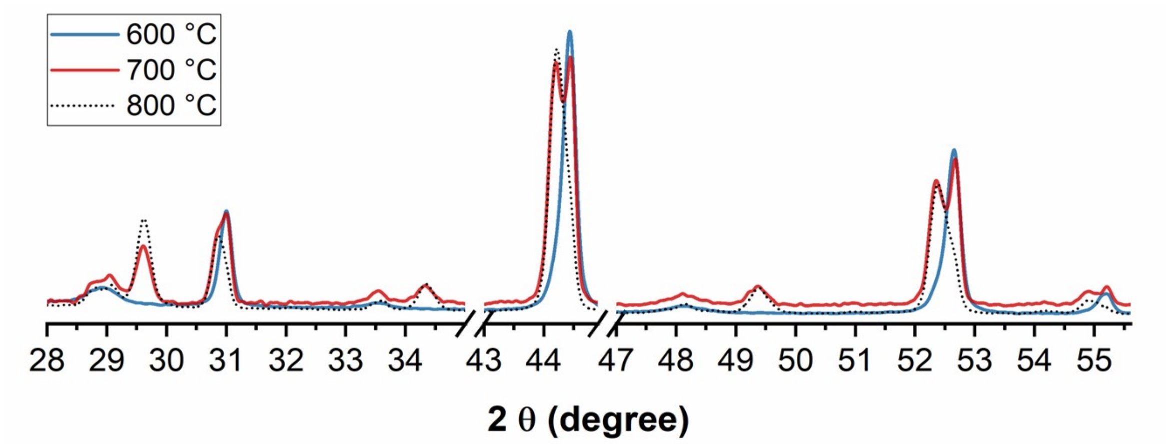

Figure S12: XRD-pattern of UCNC-700 compared to UCNC-600 and UCNC-800; UCNC-700 shows that upon calcination for 3h at 700 ◦C there is a mix between the $Sr_{0.89}Yb_{10}Er_{0.01}F_{2.11}$-phase and the oxygenized phase.

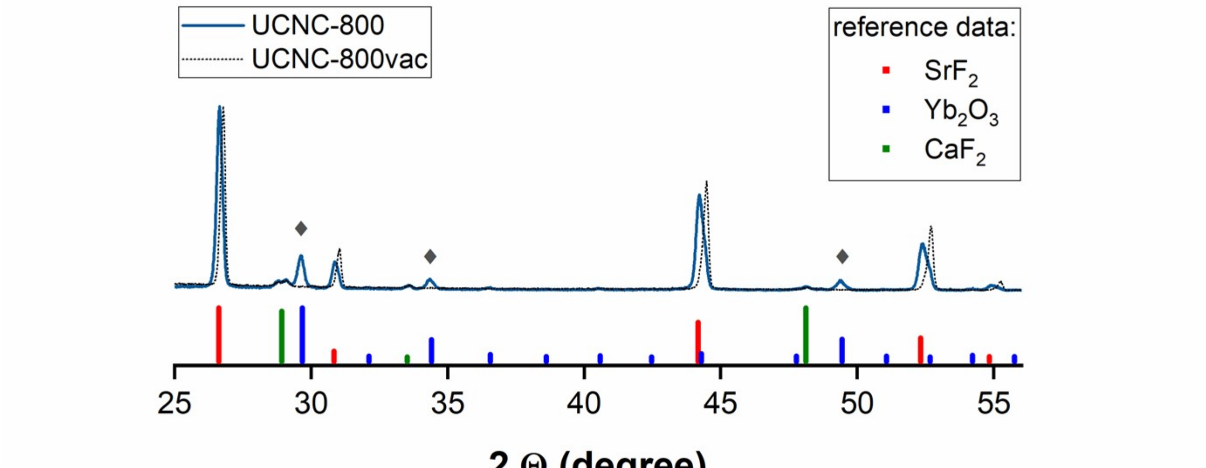

Figure S13: XRD-pattern of UCNC-800 calcinated in air and UCNC-800vac calcinated in vacuum ompared to reference patterns of SrF_2, Yb_2O_3 and Ca F_2; In addition to the reflections of SrF_2, reflections of Yb_2O_3 and CaF_2 are also present in UCNC-800; calcinating at vacuum conditions prevents the formation of oxide

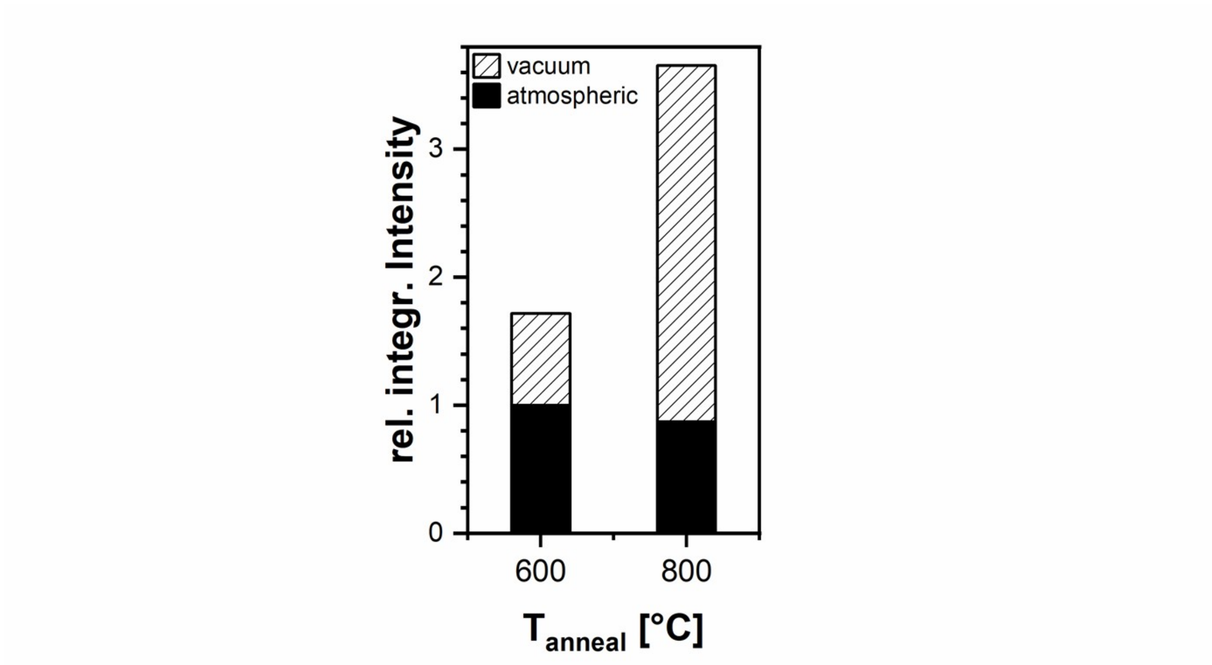

Figure S14: Relative integrated UCL intensities of UCNC powders annealed at 600 °C and 800 °C under atmospheric and vacuum conditions. Annealing under atmospheric conditions leads decreasing UCL when annealing above 600 °C due to oxygenation. By vacuum annealing significantly higher UCL can be achieved due to the prevention of the oxygenation of the lanthanide ions.

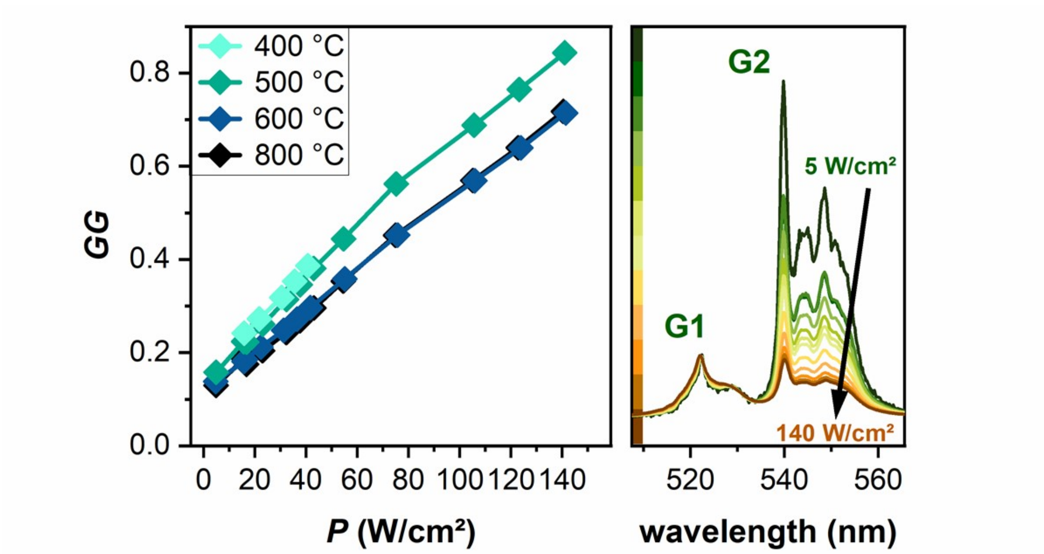

Figure S15*:* (left) *P*-dependent *GG*-Ratio of UCNC powders: UCNC-400, UCNC-500, UCNC-600 and UCNC-800. (left). The *GG*-Ratio is the quotient of the two green emitting transitions $^{2}H_{11/2} \rightarrow {}^{4}I_{15/2}$ and $^{4}S_{3/2} \rightarrow I_{15/2}$ (G1,G2) with G1 as numerator and G2 as denominator. (right) exemplary evolution of the green emission bands ($^{2}H_{11/2}$,$^{4}S_{3/2} \rightarrow {}^{4}I_{15/2}$) of UCNC-500.

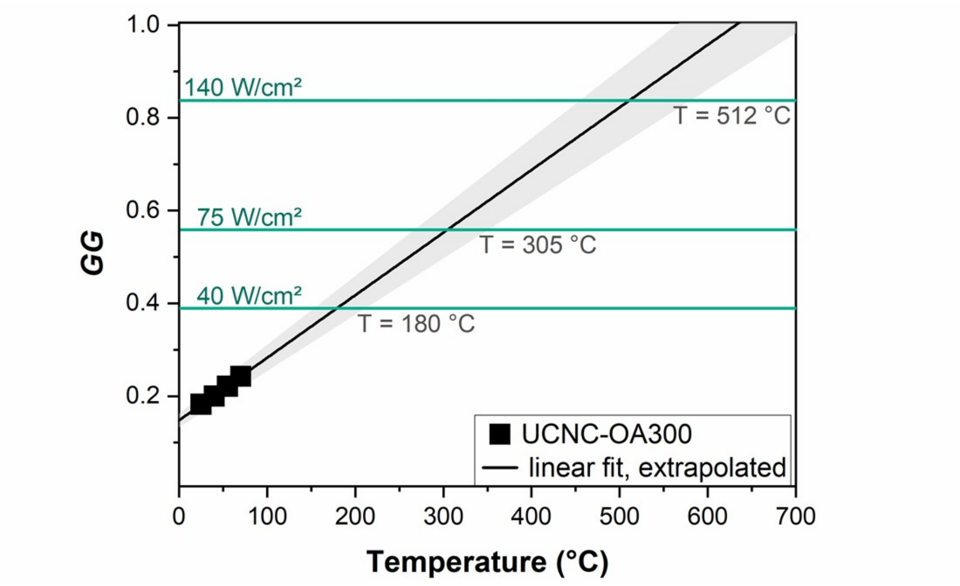

Figure S16: Thermometric calibration curve of SrF_2:$Yb_{10}Er_1$ UCNC dispersion annealed in oleic acid/octadecene at 300°C (OA300); linear fit extrapolated to high GG corresponding to value range determined in S15; exemplary GG values of S15 at various *P* represented as horizontal lines, determined temperatures noted

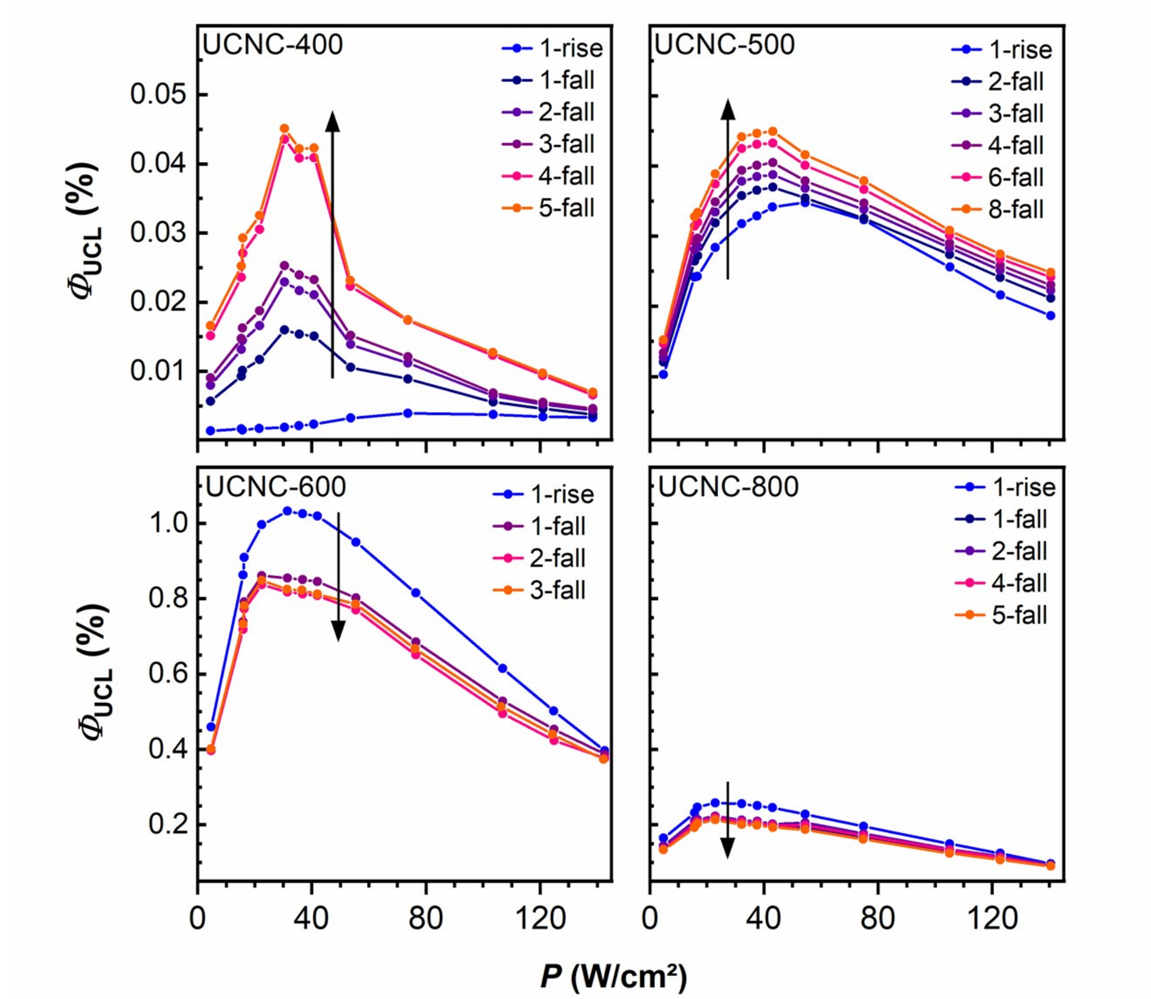

Figure S17: Calcination effect observed upon applying multiple laser irradiation cycles in the integrating sphere using a 8W 976 nm laser diode; *P*-dependent Φ_{UCL} of UCNC-400 (top, left) and UCNC-500 (top,right), UCNC-600 (bottom,left) and UCNC-800 (bottom, right)

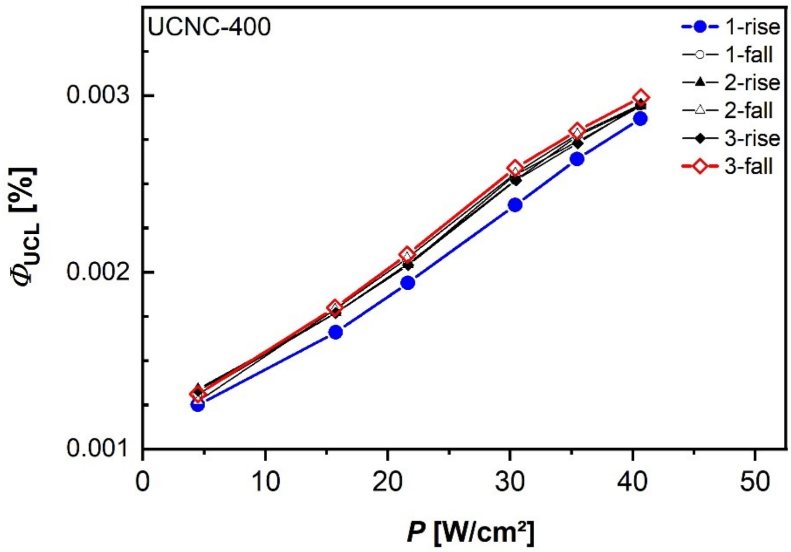

Figure S18: *P*-dependent Φ_{UCL} of UCNC-400 upon applying three laser irradiation cycles at λ_{ex} = 976 nm in the low *P* range (5 to 40 W/cm²); Noted in the legend as rise and fall, each cycle is divided into increasing *P* (closed symbol) and decreasing *P* (open symbol); The increasing part of the first cycle is marked in blue, and the decreasing part of the third cycle is marked in red. The data shows the reversibility of Φ_{UC} within the low *P* range demonstrating negligible heating effect on the sample, especially when comparing to UCNC-400 in Fig. S18. According to *GG*-ratios for this *P* range, the powders heat up to temperatures of 180 °C (Fig. S15, Fig. S16).